

Propagation mechanism of water-bearing cracks in deep rock mass under blasting disturbance

Based on the principle of fracture mechanics, this paper studies the mechanical model of water-bearing crack development in deep rock mass under blasting disturbance, and derives the expression of the dynamic and static coupling strength of the rock mass. In the meantime, the crack initiation and propagation of tensile shear and compressive shear cracks were investigated to disclose the effect of blasting disturbance, water pressure, geostress and crack angle on crack propagation, and to obtain the formula of crack propagation length. The formula was implemented in a case study. The results show that, in tensile-shear fracture, the geostress accelerates the crack propagation in the same direction; in compressive-shear fracture, the crack inclination angle of the position most vulnerable to compressive-shear fracture varies with the internal friction angle of the rock mass; the blast disturbance load, in a certain sense, elevates the water pressure in the cracks; the crack propagation length decreases in a near linear pattern with the increase in the distance from the explosion source.

Keywords: *Static and dynamic coupling, stress intensity factor, fracture toughness, equivalent blasting disturbance load.*

1. Introduction

High geostress and head pressure are inevitable issues in deep mining. The previous studies have shown that the two issues play a non-negligible role in the crack initiation and propagation within the surrounding rocks [1-4]. For safe mining, it is important to study the cracking and propagation of water-bearing cracks with blasting disturbance under high geostress.

Much research has been done on the initiation and propagation mechanism of water-bearing cracks in deep rock mass, yielding some meaningful results. For example, Wong et al.[5-6] conducted theoretical research and indoor/outdoor

tests on the influencing factors of crack fracture, concluding that the internal friction coefficient, surrounding rock and surrounding strain field are the local determinants of crack initiation. Kemeny et al.[7] argued that the stress intensity factor at the crack tip consists of stress intensity factors generated by crack water pressure, shear stress, confining pressure, etc., and established a fracture model of rock under water pressure. Galybin et al.[8] held that the stress wave tends to form a local stress balance, so that the crack deviates from the initial cracking direction. Dyskin et al.[9] created a numerical model of crack fracture in a 3D environment, and explored the effects of crack direction and depth variation on crack propagation morphology. Through tests on rock stress and strain, Souley et al.[10] attributed the macroscale propagation of cracks mainly to the evolution of rock microstructure. Weijers et al.[11] applied the Biot-Savart law to study the cracking and closure of rock fractures under different pressures. To sum up, the above scholars have probed into the composition of the stress intensity factors and the occurrence of the crack initiation, and gained initial insights into the influencing factors of crack fracture. However, there is rarely any report on the coupled effect of dynamic and statics factors on cracks.

With respect to the role of water, Dunning et al. [12] regarded the water within the rock mass an aqueous solution that induces microscale water-rock interaction, and alters the mechanical properties of the rock mass on the macroscale. Bruno et al. [13] found that the crack propagation is promoted by an increase in water pressure, but hindered by the gradient variation of water pressure. Numerical simulation was conducted by Li [14], Thallak [15] et al. to reveal the fracture process of rocks under variable water pressure. Similarly, Min et al. [16] put forward a compressive shear model of rocks under water pressure by numerical simulation, pointing out that the negative correlation between permeability and stress growth turns positive after the compressive shear fracture. Louis [17] carried out coupling experiments on crack water pressure and normal stress, and discovered the exponential negative correlation between crack permeability and the normal stress growth. Esaki et al. [18] developed an experimental system for compressive shear of cracks under water pressure, and discovered that the rock permeability

Messrs. Xiaoming Lou and Congcong Wang, Zijin Mining College, Fuzhou University, Fuzhou 350 116 and also with Institute for Explosive Technology, Fuzhou University, Fuzhou 350 116 and Wenbin Jian, Institute of Geotechnical and Geological Engineering, Fuzhou University, Fuzhou 350 116, China. E-mail: Xiaoming Lou; 331261323@qq.com

increased by two orders of magnitude after the compressive shear fracture of cracks. These studies, mainly concentrated in the effect of water pressure on rock mechanics and the relationship between rock permeability and crack fracture, have identified the preliminary relationship between rock permeability and rock mechanics. Unfortunately, there is insufficient quantitative research into the effect of water pressure on crack fracture.

As for the theoretical models on fracture Oda [19] examined the coupling effects of seepage field and stress field under water pressure, and established an equivalent continuum model of crack fracture. Using fracture mechanics, Adachi et al. [20] studied the plane stress and strain of the crack tip in water-bearing fracture process. Similarly, Zhao et al. [21] studied the microscale fracture mechanism of rock cracks under high water pressure, and proposed a calculation model for wing-shaped crack propagation. Sih et al. [22] explored the stress field and displacement field of the crack tip under dynamic loads, found the time-varying nature of stress factors and the consistency between the field distribution under dynamic loads with that under static loads. In addition, Liu et al. [23] redefined the opening of the crack as the sum of a soft part and a hard part, and constructed an exponential fracture model of crack opening. Noorishad et al. [24] developed a fracture model with solid-liquid coupling in discontinuous media, and elucidated the coupling relationships of each stress. These works are beneficial to the understanding of the stress field and the fracture model around crack sections in variable conditions, laying the basis for crack fracture mechanism and the calculation model. There is still much room for research into the crack fracture model under the coupling effect of static and dynamic loads.

Based on the previous studies on the initiation and propagation of water-bearing rock cracks and the influencing factors of crack fracture, this paper discusses the detailed effects of initial geostress, blasting disturbance, water pressure and physical characteristics of cracks on crack propagation, aiming to disclose the initiation and propagation of water-bearing rock cracks under high geostress and high water pressure.

2. Calculation of stress intensity factor

The propagation of water-bearing cracks in deep rock mass is constrained by such external factors as the initial geostress, water pressure and blasting disturbance load. In light of this, the author established the calculation model of water-bearing cracks in deep rock mass (Fig.1).

It is assumed that any crack is affected by both vertical stress σ_1 and horizontal stress σ_3 (the crack angle, i.e., the angle between the crack and the vertical stress is β), water pressure P , and blasting disturbance (P , SV stress wave). Under the joint action of these factors, the crack starts to expand at the initiation angle of θ (Fig.2).

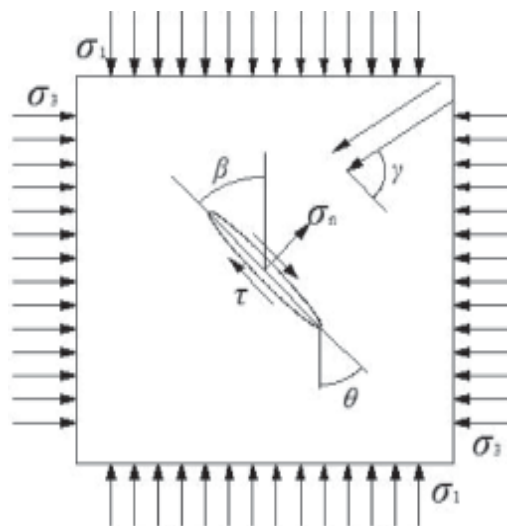


Fig.1 Calculation model of water-bearing cracks in deep rock mass

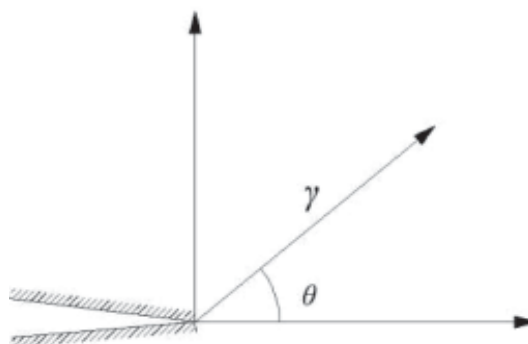


Fig.2 Polar coordinates at the crack tip

When the crack propagation is affected by various factors and follows the same propagation pattern, the stress intensity factor at the crack tip equals the algebraic sum of each factor [5-6]. In fact, the crack propagation is driven concertedly by the dynamic loads of blasting disturbance and the static loads of initial stress and water pressure. Therefore, the dynamic stress factor and the static stress factor were employed to represent the coupling stress factor of the water-bearing crack tip in deep rock mass under blasting disturbance.

$$K_e = K_{es} + K_{ed} \quad \dots (1)$$

where K_e is the coupling stress intensity factor; K_{es} is the static stress intensity factor; K_{ed} is the dynamic stress intensity factor.

In Fig.1, the static stresses around the cracks include geostress and water pressure. Since the two factors are constant at a fixed point (r, θ) during blasting, the static stress intensity factor was assumed to be constant in the calculation. According to the principle of fracture mechanics, the tensile stress is positive and the compressive stress is negative in the formula. Hence, the static stress intensity factors and can be calculated by the following formula [25].

... (2)

The explosive stress wave can be divided into P wave and SV wave after blasting. Because SV wave produces a greater dynamic stress intensity factor than P wave at the crack tip [26], this research mainly considers the effect of SV wave on crack propagation. According to the propagation law of SV wave, the dynamic stress intensity factors K_I and K_{II} generated at the crack tip are time-variants:

$$\left. \begin{aligned} K_I' &= \mu v \sqrt{\pi a} |K_I^{(2)}| \exp[-iw(t - \delta_1)] \\ K_{II}' &= \mu v \sqrt{\pi a} |K_{II}^{(2)}| \exp[-iw(t - \delta_2)] \end{aligned} \right\} \quad \dots (3)$$

where μ is the Lamé constant; v is the peak vibration velocity of the incident wave; $|K_I^{(2)}|$ and $|K_{II}^{(2)}|$ are the dynamic stress intensity factors of magnitude 1; δ_1 and δ_2 are the phase angles.

The maximum effect of dynamic stress intensity factors on crack propagation was obtained based on the maximum value of these factors:

$$\left. \begin{aligned} K_I' &= \mu v \sqrt{\pi a} |K_I^{(2)}| \\ K_{II}' &= \mu v \sqrt{\pi a} |K_{II}^{(2)}| \end{aligned} \right\} \quad \dots (4)$$

3. Analysis on initiation and propagation of water-bearing cracks

As shown in Fig.1, when the crack normal stress σ_n is a tensile force, the cracks propagate as the mixture of type I-II tensile-shear cracks; when the normal stress σ_n is a pressure force, the crack propagate as the mixture of type I-II compressive-shear cracks. Thus, the fracture of type I-II compound cracks should be studied from the angles of tensile-shear fracture and compressive-shear fracture.

3.1 TENSILE-SHEAR CRACK

3.1.1 Crack initiation

The approximate fracture criterion was adopted for tensile-shear fracture [27], that is, the fracture criterion of I-II tensile-shear cracks can be expressed as:

$$K_{ID} = \left\{ P - \left(\frac{\sigma_1 + \sigma_3}{2} - \frac{\sigma_1 - \sigma_3}{2} \cos 2\beta \right) - \left| \frac{\sigma_1 - \sigma_3}{2} \sin 2\beta \right| + \mu v \left(|K_I^{(2)}| + |K_{II}^{(2)}| \right) \right\} \sqrt{\pi a} \quad \dots (5)$$

where K_{ID} is the dynamic fracture roughness of type I cracks; K_I and K_{II} are the static stress intensity factors of type I and II cracks, respectively; K_I' and K_{II}' are the dynamic stress intensity factors of crack type I and II, respectively.

The lateral pressure coefficient λ ($\lambda = \sigma_3/\sigma_1$) of geostress was introduced to describe the fracture criterion. Hence, Equation (5) can be transformed as:

... (6)

If the equivalent blasting disturbance is defined as

$\sigma' = \mu v \left(|K_I^{(2)}| + |K_{II}^{(2)}| \right)$ at the occurrence of tensile-shear fracture, then σ' and crack water pressure P exert a synergistic effect on crack initiation. The stress intensity factors at the crack tip increase with σ' and P . The greater the factors are, the higher the probability of cracking.

The relationships among equivalent disturbance load, crack inclination, and lateral geostress coefficient can be derived according to Table 1 and Equation (6).

In Fig.3, the negative values of the equivalent blasting disturbance is attributable to the crack propagation under the presence of water pressure P , which, together with equivalent blasting disturbance load σ' , induced the initiation of cracks. According to Figs.3 and 4, the equivalent blasting disturbance leading to crack initiation varied symmetrically on the two sides of 90° inclination. In the range of 0° to 45°, the equivalent blasting disturbance load σ' increased with the value of λ , adding to the difficulty in cracking. In the range of 45° to 90°, σ' decreased with the increase of λ when $\lambda < 1$, making it easier for the rock to crack, but increased with λ when $\lambda > 1$, making it more difficult for the rock to crack.

TABLE 1: CALCULATION PARAMETERS FOR CRACK INITIATION OF TENSILE-SHEAR FRACTURE [25]

Parameters	v	E (GPa)	μ'	a (m)	K_{IC} (MN/m ^{3/2})	K_{IIC} (MN/m ^{3/2})
Values	0.25	30	0.58	1	15.2	11.2

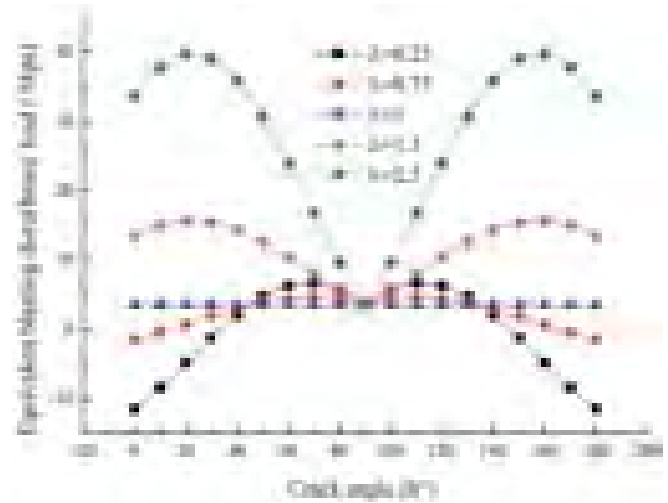


Fig.3 Relationship of equivalent blasting disturbance load and crack inclination

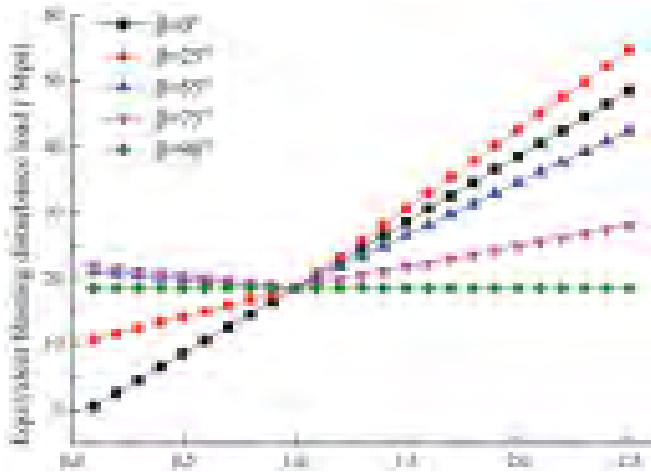


Fig.4 Relationship of equivalent blasting disturbance load and lateral geostress coefficient

It is also observed that the equivalent blasting disturbance load σ' is closely related to the change of the lateral geostress coefficient. When $\lambda < 1$, σ' reached the minimum when $\beta = 0^\circ$, indicating that vertical cracking occurred when the vertical stress surpassed the horizontal stress. When $\lambda = 1$, σ' remained constant whichever the crack angle, revealing that the horizontal geostress was equal to the vertical stress, and that they affected the crack in the same pattern. When $\lambda > 1$, σ' reached the minimum at $\beta = 90^\circ$, showing that the cracks tended to expand in the horizontal direction when the vertical stress was below the horizontal geostress. In summary, the cracks are more likely to initiate and propagate when the angle is relatively small between the crack direction and the direction of the greater geostress.

Equation (6) can be modified as follows to fully demonstrate the initiation factors of water-bearing cracks in deep rock mass, and further simplify the fracture criterion of tensile-shear crack:

$$\frac{P + \sigma' - \frac{K_{ID}}{\sqrt{\pi a}}}{\sigma_1} = \frac{1 + \lambda}{2} - \frac{1 - \lambda}{2} \cos 2\beta + \frac{|(1 - \lambda) \sin 2\beta|}{2} \quad \dots (7)$$

In fact, the non-dimensional quantity on the right side of Equation (7) reflects the effect of lateral geostress coefficient and crack inclination on crack initiation. If the quantity is denoted as m , then the generalized fracture criterion of the tensile-shear fracture can be expressed as:

$$(P + \sigma' - m\sigma_1)\sqrt{\pi a} = K_{ID} \quad \dots (8)$$

3.1.2 Crack propagation

According to the crack arrest principle [26], the arrest of cracks depends on the arrest toughness. Considering the speed of crack propagation, the arrest toughness is divided into dynamic arrest toughness K_{ID} and static arrest toughness K_{IC} . If the K_{ID} is too difficult to obtain, it can be regarded as equal to K_{IC} . Focusing on the effect of blasting wave on crack propagation in far away areas, this research

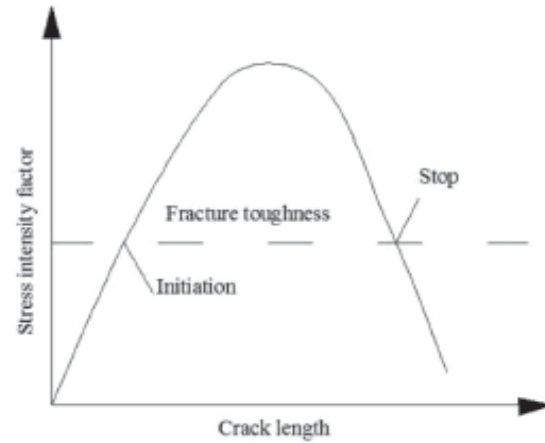


Fig.5 Conditions of crack arrest

takes the static arrest toughness K_{IC} as critical arrest condition (Fig.5).

In the process of crack propagation, the vibration velocity and frequency of stress wave attenuated with the increase in the distance from the explosion source, leading to a decline of dynamic stress intensity factors. The cracks were arrested when the dynamic stress intensity factors reached the critical value. Assuming that the crack propagation length is Δl , the angle between the crack and the stress wave is γ and the initiation angle is θ , the stress wave propagation distance ΔR in the range of Δl can be expressed as follows:

$$\Delta R = R + \Delta l \cdot \cos\left(\frac{\pi}{2} + \theta - \gamma\right) \quad \dots (9)$$

where R is the distance between the explosion source and the crack centre. According to the modified Sadovsky formula [28], the attenuation of the vibration velocity can be expressed as:

$$v = KQ^{\frac{\alpha}{3}} \left[R + \Delta l \cdot \cos\left(\frac{\pi}{2} + \theta - \gamma\right) \right]^{-\alpha} \quad \dots (10)$$

where K and α are the attenuation coefficients. Based on Equations (8)~(10), the crack propagation length can be calculated by:

$$\frac{K_{IC}}{\sqrt{\pi a}} = P + \mu K Q^{\frac{\alpha}{3}} \left[R + \Delta l \cdot \cos\left(\frac{\pi}{2} + \theta - \gamma\right) \right]^{-\alpha} \times \left(\begin{matrix} |K_I^{(2)}| \\ + |K_{II}^{(2)}| \end{matrix} \right) - m\sigma_1 \quad \dots (11)$$

According to the monitoring of the vibration velocity attenuation in an underground project, the attenuation coefficients in the vibration velocity attenuation function are $K=663.385$, $\alpha=1.929$. Then, the vibration attenuation formula can be obtained according to Equation (9). Considering the $|K_I^{(2)}|$ and $|K_{II}^{(2)}|$ in certain conditions [26], it is possible to deduce the relationship between distance to explosion source and the equivalent blasting disturbance load, as well as the regularity of the crack propagation length under various lateral geostress coefficients (Figs.6-7).

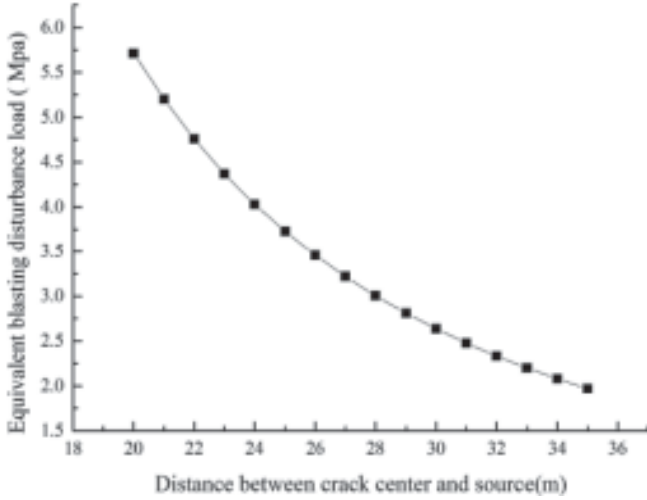


Fig.6 Attenuation of equivalent blasting disturbance load

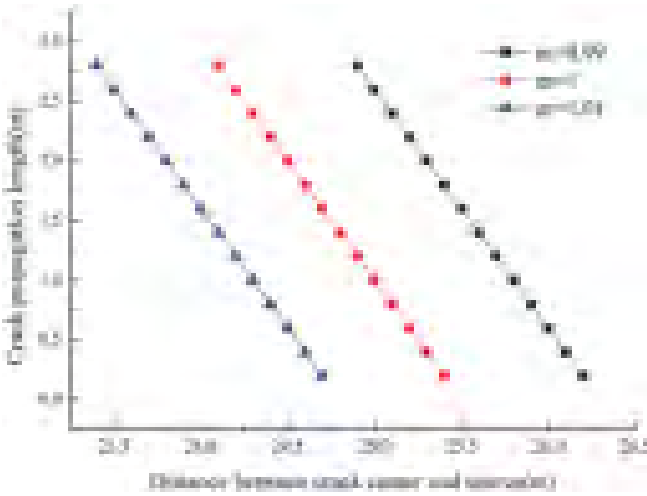


Fig.7 Length of crack propagation

The velocity of blasting vibration decreased with the increase in the distance from the explosion source, resulting a decrease in the equivalent disturbance load. Similarly, the length of crack propagation almost linearly decreased with the increase in that distance (Fig.7). When the crack propagation length is zero, the cracks remain in their critical fracture state, and the positions of cracks form the scope of blasting influence on cracking. In addition, when m is 0.99 ~ 1.01, the scope of blasting influence on the tensile-shear fracture is 24.75 ~ 26.25 m (Fig.7).

3.2 COMPRESSIVE-SHEAR CRACK

3.2.1 Crack initiation

The maximum circumferential stress criterion was adopted to analyse the compressive-shear fracture [29-30]. The circumferential stress at the point (r, θ) in the polar coordinate system (Fig.2) can be expressed as:

$$\sigma_{\theta} = \frac{1}{2\sqrt{2\pi r}} \cos \frac{\theta}{2} \left[3\sin \theta (K_{II} + K_{II}') - (K_I + K_I')(1 + \cos \theta) \right] \quad \dots (12)$$

Let the stress intensity factors $K_I = K_{II} = 0$ for the compressive-shear fracture, and the crack initiation angle of the compressive-shear crack be 70.5° [26]. Then, the fracture criterion of the I-II compressive-shear crack can be expressed as:

$$K_{III} = \frac{2\sqrt{3}}{3} (K_{II} + K_{II}') \quad \dots (13)$$

As the normal stress σ_n of the crack surface becomes pressure, the crack is closed and the σ_n produces friction on the crack surface, changing the shear stress of the crack surface [25]:

$$\tau' = |\tau| - (\mu' \sigma_n + c) \quad \dots (14)$$

where μ' is the friction coefficient; c is the cohesive force of the crack surface ($c = 0$).

For the compressive-shear fracture, the compressive stress is positive. According to Equations (2), (4), (13) and (14), the fracture criterion of crack fracture can be expressed as:

$$K_{III} = \frac{2\sqrt{3}\pi a}{3} \left[\begin{array}{l} \mu' P + \mu \nu |K_{II}^{(2)}| + \left| \frac{\sigma_1 - \sigma_3}{2} \sin 2\beta \right| \\ -\mu' \left(\frac{\sigma_1 + \sigma_3}{2} - \frac{\sigma_1 - \sigma_3}{2} \cos 2\beta \right) \end{array} \right] \quad \dots (15)$$

Similarly, Equation (15) can be transformed as:

$$\mu' P + \mu \nu |K_{II}^{(2)}| = \frac{\sqrt{3}K_{III}}{2\sqrt{\pi a}} + \sigma_1 \left[\begin{array}{l} \mu' \left(\frac{1+\lambda}{2} - \frac{1-\lambda}{2} \cos 2\beta \right) \\ - \frac{|(1-\lambda) \sin 2\beta|}{2} \end{array} \right] \quad \dots (16)$$

If the equivalent blasting disturbance is defined as $\sigma'' = \mu \nu |K_{II}^{(2)}|$ at the occurrence of compressive-shear fracture, then σ'' and crack water pressure P also exert a synergistic effect on crack initiation. The stress intensity factors at the crack tip increase with σ'' and P . The greater the factors are, the higher is the probability of cracking.

The relationships among equivalent disturbance load, crack inclination, and lateral geostress coefficient can be derived according to Table 1 and Equation (16). The relationships among σ'' , crack angle and geostress are displayed in Figs.8 and 9.

In Figs.8-9, the negative values of the equivalent blasting disturbance load is attributable to the crack propagation under the presence of water pressure P which, together with equivalent blasting disturbance load σ'' , induced the initiation of cracks. Moreover, the equivalent blasting disturbance leading to crack initiation varied symmetrically on the two sides of 90° inclination. In the range of 0° to 30° , the equivalent blasting disturbance load σ'' increased with the value of λ , adding to the difficulty in cracking. In the range of 30 to 90° , σ'' still increased λ when $\lambda < 1$, making it more difficult for the rock to crack, but decreased with the increase

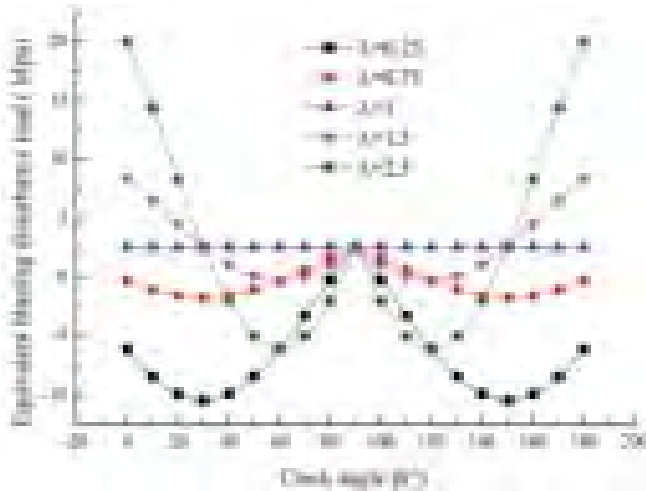


Fig.8 Relationship between equivalent blasting disturbance loading and crack inclination

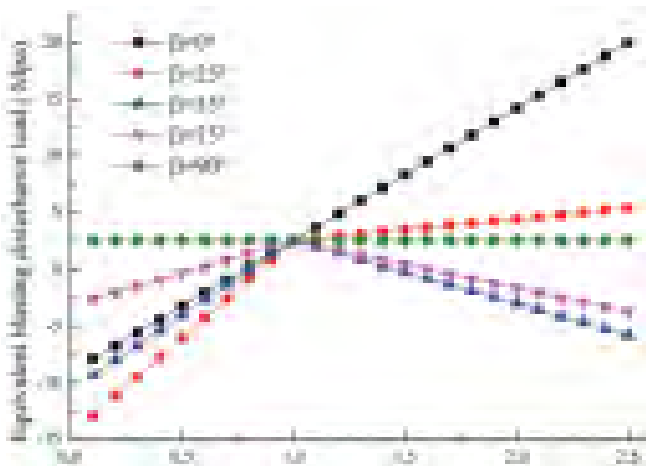


Fig.9 Relationship between equivalent blasting disturbance load and lateral stress coefficient

of λ when $\lambda > 1$, making it easier for the rock to crack.

When the internal friction coefficient was 0.58, the equivalent blasting disturbance load reached the minimum at $\beta = 30^\circ$ when $\lambda < 1$, indicating that the crack with a 30° inclination angle is prone to failure when the vertical stress was greater than the horizontal stress. When $\lambda = 1$, σ'' remained constant whichever the crack angle, revealing that the horizontal geostress was equal to the vertical stress, and that they affected the crack in the same pattern. When $\lambda > 1$, σ'' reached the minimum at $\beta = 60^\circ$, showing that the crack with a 60° inclination angle is prone to failure when the vertical stress was smaller than the horizontal stress.

The relationship between the internal friction coefficient μ' and the internal friction angle φ of the rock mass obeys $\mu' = \tan \varphi$. Therefore, the authors established the relationships among the critical equivalent disturbance load, the crack angle, and the lateral geostress coefficient at various internal friction angles (Fig.10).

As shown in Fig.10, the crack inclination angle of the position most vulnerable to compressive-shear failure varies with the internal friction angle of the rock mass. When the internal friction angle fell in the range of 10° - 80° , the said crack inclination angle varied from 40° to 50° in a rock mass with lateral geostress coefficient $\lambda > 1$, and from 50° to 85° in a rock mass with lateral geostress coefficient $\lambda < 1$. There was still a linear relationship between the said inclination angle and the lateral geostress coefficient.

Equation (16) can be modified as follows to fully demonstrate the initiation factors of water-bearing cracks in deep rock mass:

$$P + \frac{\mu\nu |K_{II}^{(2)}|}{\mu'} - \frac{\sqrt{3}K_{III}}{2\mu'\sqrt{\pi a}} = \frac{1+\lambda}{2} - \frac{1-\lambda}{2} \cos 2\beta - \frac{|(1-\lambda)\sin 2\beta|}{2\mu'} \dots (17)$$

If the non-dimensional quantity on the right side of Equation (7) is denoted as m' , then the generalized fracture criterion of the compressive-shear fracture can be expressed as:

$$\left(P + \frac{\sigma'}{\mu'} - m'\sigma_1 \right) \sqrt{\pi a} = \frac{\sqrt{3}K_{III}}{2\mu'} \dots (18)$$

3.2.2 Crack propagation

Similar to the calculation of the tensile-shear crack length, the fracture toughness was $K_{IIC} = K_{IIC}$. Then, the shear crack propagation length can be expressed as:

$$\frac{\sqrt{3}K_{IIC}}{2\mu'\sqrt{\pi a}} = P + \frac{\mu K Q^{\frac{\alpha}{3}} \left[R + \Delta l \cos \left(\frac{\pi}{2} + \theta - \gamma \right) \right]^{-\alpha} |K_{II}^{(2)}|}{\mu'} - m'\sigma_1 \dots (19)$$

According to the parameters and calculation methods of the length in the tensile-shear crack propagation, the relationships between the distance from the explosion source and the equivalent blasting disturbance as well as the crack propagation length under different lateral pressure coefficients are shown in Figs.11-12.

In Fig.11, the equivalent blasting disturbance load decreased with the increase in the distance from the explosion source. In Fig.12, however, the disturbance load and the propagation length of the compressive-shear crack both decreased linearly with the increase in the distance from the explosion source in the given rock mass. Overall, the scope of blasting influence on the compressive-shear fracture is 9.5~10.9 m when $m' = 0.9 \sim 1.1$.

4. An example of fracture calculation

In this section, the LS-DYNA dynamic finite-element software was adopted to simulate the vibration and stress attenuation law after the concentrated blasting of single packs. Considering the structural symmetry, 1/4 model was selected for further analysis. The two vertical sides of the rock were symmetrically constrained, and the non-reflective boundary

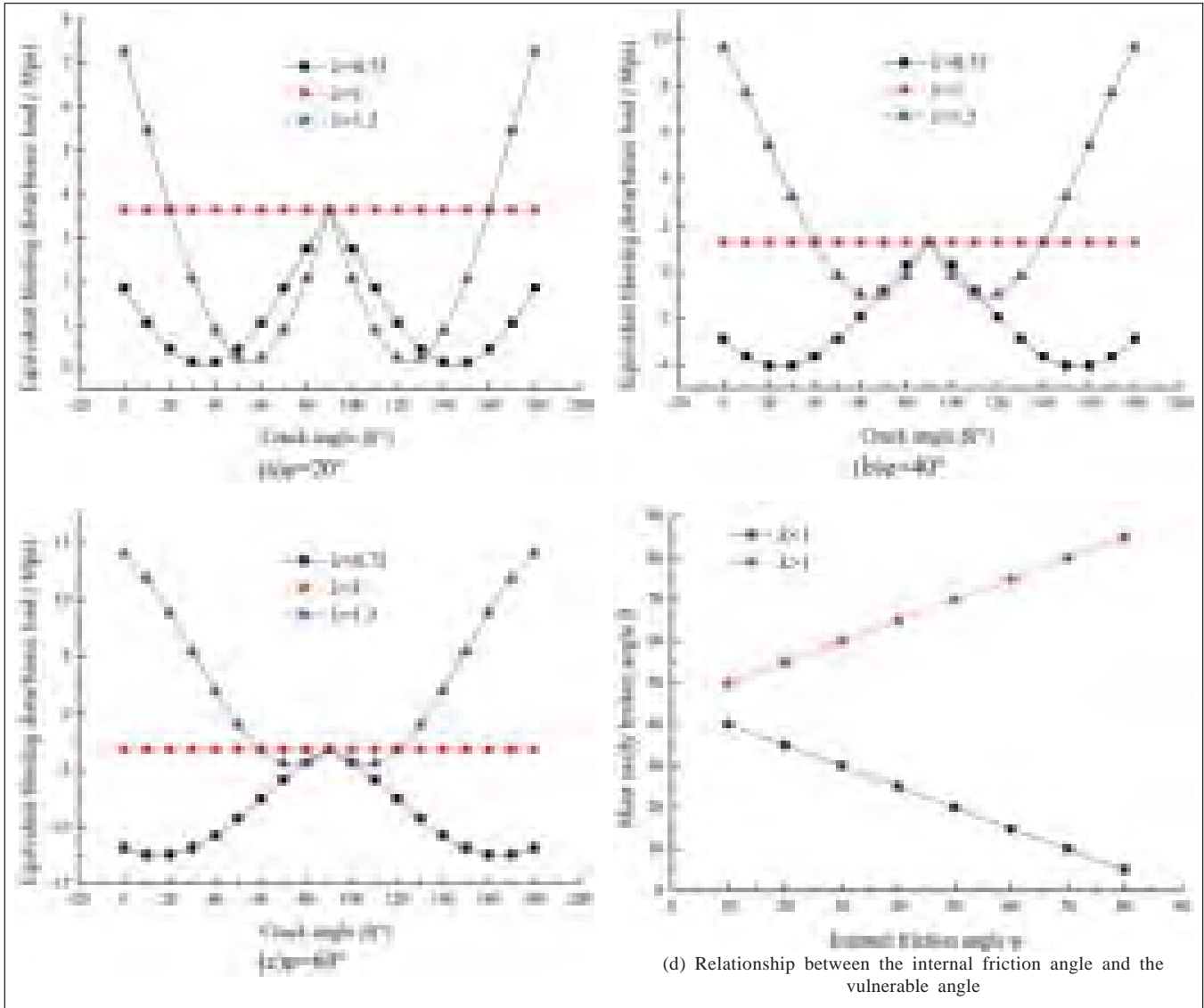


Fig.10 Relationship between the vulnerable angle and the internal friction coefficient

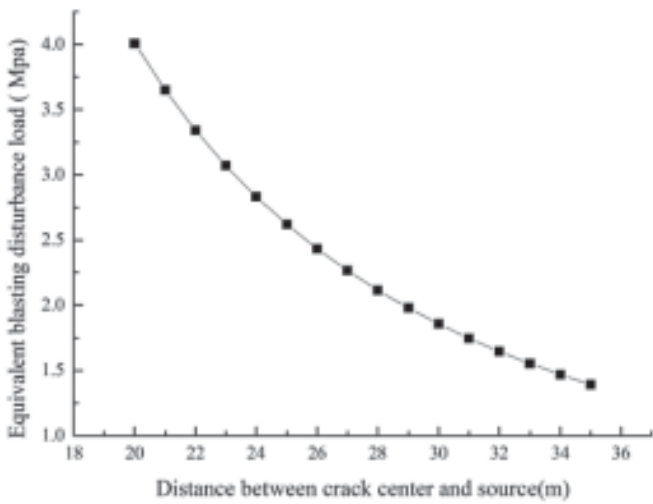


Fig.11 Attenuation of equivalent disturbance load

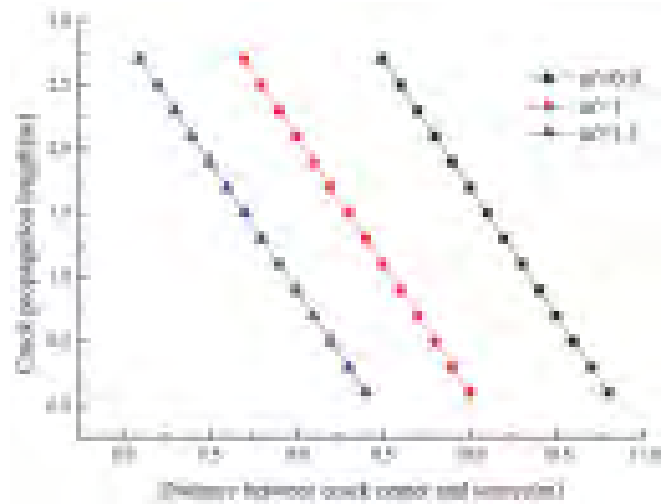


Fig.12 Length of crack propagation

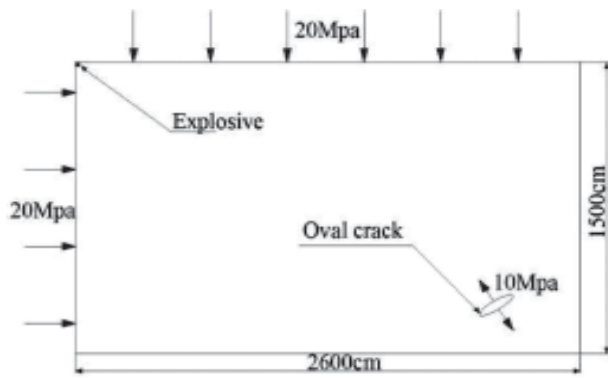


Fig.13 Model size and applied force

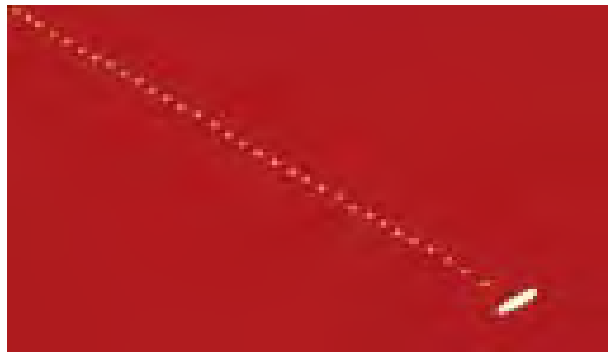


Fig.14 Length of crack propagation

is applied in four directions to simulate the infinite rock mass. The size of the 1/4 solid rock model is 2,600cm long and 1,500cm high, and a 100cm-long elliptical crack was set at 2,500cm away from the borehole. To simulate the stress condition of water-bearing cracks in deep rock mass, an implicit-explicit transformation was introduced to apply a static deep geostress of 20MPa on the top and left side of the model, and a static water pressure 10MPa in the crack. The disturbance of explosives on the crack was simulated by the flow-solid coupling algorithm. The explosive was modelled with MAT-HIGH-EXPLOSIVE-BURN material, and the relationship between pressure and volume during explosion was simulated by EOS-JWL state equation. The calculation model and measuring points arrangement are shown in Figs.13 and 14.

The relationship of the blasting vibration velocity and the distance from the explosion source is depicted Fig.15. With the increase in the distance from the source, the vibration velocity generally exhibited a declining trend. The attenuation amplitude of the vibration velocity was 77.7~9.8 cm/s at 1~25 m away from the explosion source. Moreover, the relationship of the equivalent blasting disturbance load and the distance from the source is recorded in Fig.16. As shown in the figure, the equivalent perturbation load declined with the increase in the distance from the explosion source. The descend range was 11.4~1.5 MPa at 1~25m away from the explosion source. The simulated attenuation curves are consistent with the

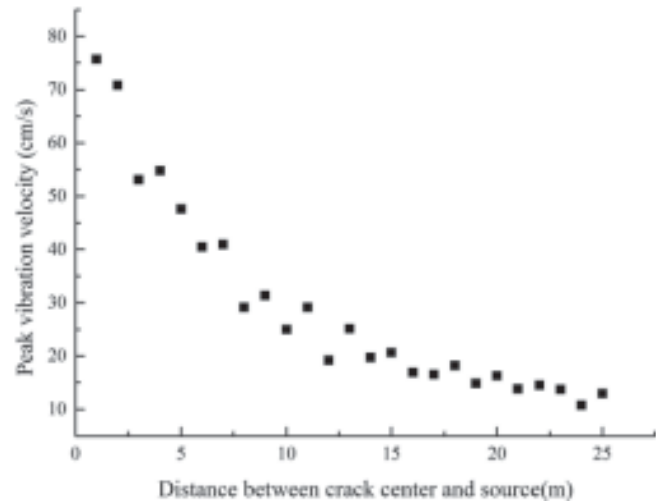


Fig.15 Attenuation of vibration velocity

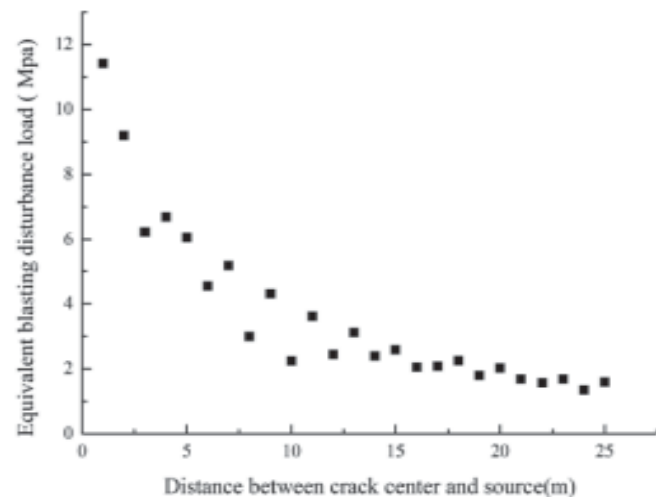


Fig.16 Attenuation of equivalent disturbance load

results in Figs.6 and 11, and thereby verify the accuracy of the theoretical study.

5. Conclusions

- (1) The blasting disturbance load, in a certain sense, elevates the water pressure in the cracks. The cracks suffer from tensile-shear crack when the coupling effect of the blasting disturbance load and the water pressure exceeds the geostress on the cracks, and compressive-shear crack when the coupling effect is lower than the geostress.
- (2) For the tensile-shear fracture, it is easier for the crack to propagate when the crack direction points to the direction with the greater geostress. For the compressive-shear fracture, the crack inclination angle of the position most vulnerable to compressive-shear fracture varies with the internal friction angle of the rock mass. For both fracture patterns, the degree of difficulty in crack fracture is stratified by the lateral stress coefficient $\lambda=1$. However, the degree of difficulty evolves oppositely in the two patterns

according to the lateral stress coefficients.

- (3) With the increase in the distance from the explosion source, the stress wave of blasting continues to attenuate, and the equivalent disturbance load has an increasingly small effect on crack initiation and propagation. Moreover, the crack propagation length decreases in a near linear pattern with the increase in the distance from the explosion source.

Acknowledgment

It is gratefully noted that the work is supported by The National Natural Science Foundation of China.(No. 41072232).

References

1. Bohlooli, B. and Pater, C. J. D. (2006): "Experimental study on hydraulic fracturing of soft rocks: Influence of fluid rheology and confining stress." *Journal of Petroleum Science & Engineering*, vol. 53, no. 1, pp. 1-12.
2. Cappa, F., Guglielmi, Y., Fénart, P., Merrien-Soukatchoff, V. and Thoraval, A. (2005): "Hydromechanical interactions in a fractured carbonate reservoir inferred from hydraulic and mechanical measurements." *International Journal of Rock Mechanics & Mining Sciences*, vol. 42, no. 2, pp. 287-306.
3. Wu, Q., Wang, M. and Wu, X. (2004): "Investigations of groundwater bursting into coal mine seam floors from fault zones." *International Journal of Rock Mechanics & Mining Sciences*, vol. 41, no. 4, pp.557-571.
4. Wolkersdorfer, C. and Bowell, R. (2004): "Contemporary Reviews of Mine Water Studies in Europe, Part 1." *Mine Water & the Environment*, vol. 23, no. 4, pp. 162-182.
5. Wong, R. H. C. and Chau, K. T. (1997): "The coalescence of frictional cracks and the the shear zone formation in brittle solids under compressive stresses." *International Journal of Rock Mechanics & Mining Sciences*, vol. 34, no. 3-4, pp.335.
6. Wong, R. H. C., Chau, K. T., Tang, C. A. and Lin, P. (2001): "Analysis of crack coalescence in rock-like materials containing three flaws-Part I: experimental approach." *International Journal of Rock Mechanics & Mining Sciences*, vol. 38, no. 7, pp. 909-924.
7. Kemeny, J. M. (1991): "A model for non-linear rock deformation under compression due to sub-critical crack growth." *International Journal of Rock Mechanics & Mining Sciences & Geomechanics Abstracts*, vol. 28, no. 6, pp.459-467.
8. Galybin, A. N. and Dyskin, A. V. (2004): "Random trajectories of crack growth caused by spatial stress fluctuations." *International Journal of Fracture*, vol. 128, no.1-4, pp.95-103.
9. Dyskin, A. V., Sahouryeh, E., Jewell, R. J., Joer, H. and Ustinov, K. B. (2003): "Influence of shape and locations of initial 3-D cracks on their growth in uniaxial compression." *Engineering Fracture Mechanics*, vol. 70, no. 15, pp.2115-2136.
10. Souley, M., Homand, F., Pepa, S. and Hoxha, D. (2001): "Damage-induced permeability changes in granite: a case example at the URL in Canada." *International Journal of Rock Mechanics & Mining Sciences*, vol.3 8, no. 2, pp.297-310.
11. Weijers, L., Pater, C. J. and Hagoort, J. (1996): A new mechanism for hydraulic initiation. Proceedings of Rock Mechanics. Rotterdam: A. A. Balkeman.
12. Dunning, J., Douglas, B., Miller, M. and McDonald, S. (1994): "The role of the chemical environment in frictional deformation: Stress corrosion cracking and comminution." *Pure & Applied Geophysics*, vol. 143, no. 1-3, pp.151-178.
13. Bruno, M. S. and Nakagawa, F. M. (1991): "Pore pressure influence on tensile fracture propagation in sedimentary rock." *International Journal of Rock Mechanics & Mining Sciences & Geomechanics Abstracts*, vol. 28, no. 4, pp.261-273.
14. Li, L. and Holt, R. M. (2001): Simulation of flow in sandstone With fluid coupled particle model. Dc Rocks E U.s.symposium on Rock Mechanics.
15. Thallak, S., Rothenburg, L. and Dusseault, M. (1991): Simulation of Multiple Hydraulic Fractures In a Discrete Element System.
16. Min, K. B., Rutqvist, J., Tsang, C. F. and Jing, L. (2004): "Stress-dependent permeability of fractured rock masses: a numerical study." *International Journal of Rock Mechanics & Mining Sciences*, vol. 41, no. 7, pp. 1191-1210.
17. Louis, C. (1974): Rock hydraulics in rock mechanics. New York: Springer-New Verlag.
18. Esaki, T., Du, S., Mitani, Y., Ikusada, K. and Jing, L. (1999): "Development of a shear-flow test apparatus and determination of coupled properties for a single rock joint." *International Journal of Rock Mechanics & Mining Sciences*, vol. 36, no. 5, pp. 641-650.
19. Masanobu, O. (1986): "An equivalent continuum model for coupled stress and fluid flow analysis in jointed rock masses." *Water Resources Research*, vol. 22, no. 13, pp. 1845-1856.
20. Adachi, J. I. and Detournay, E. (2008): "Plane strain propagation of a hydraulic fracture in a permeable rock." *Engineering Fracture Mechanics*, vol. 75, no. 16, pp. 4666-4694.
21. Zhao, Y. L. and Wang, W. J. (2011): "Wing crack propagation model under high hydraulic pressure in compressive-shear stress state." *Journal of Coal Science and Engineering (China)*, vol.17, no.1, pp.34-38.

22. Sih, G. C. and Loeber, J. F. (1969): "Wave propagation in an elastic solid with a line of discontinuity or finite crack." *Quarterly of Applied Mathematics*, vol. 27, no. 2, pp. 193.
23. Liu, H. H., Wei, M. Y. and Rutqvist, J. (2012): "Normal-stress dependence of fracture hydraulic properties including two-phase flow properties." *Hydrogeology Journal*, vol. 21, no. 2, pp. 371-382.
24. Noorishad, J., Ayatollahi, M. S. and Witherspoon, P. A. (1982): "A finite-element method for coupled stress and fluid flow analysis in fractured rock masses." *International Journal of Rock Mechanics & Mining Sciences & Geomechanics Abstracts*, vol. 19, no. 4, pp. 185-193.
25. Li, Z. L., Zhang, H. C., Ren, Q. W. and Wang, Y. H. (2005): "Analysis of hydraulic fracturing and calculation of critical internal water pressure of rock fracture." *Rock & Soil Mechanics*, vol. 26, no. 8, pp. 1216-1220.
26. Fan, T. Y. (2006): Fracture dynamics principle and application. Beijing University of Science and Technology Press.
27. Gao, Q. (1986): Engineering fracture mechanics. Chongqing University Press.
28. Lv, T., Shi, Y. Q., Huang, C., Li, H. B. and Xia, X. (2007): "Study on attenuation parameters of blasting vibration by nonlinear regression analysis." *Rock & Soil Mechanics*, vol. 28, no. 9, pp. 1871-1878.
29. Ashby, M. F. and Hallam, S. D. (1986): "The failure of brittle solids containing small cracks under compressive stress states." *Acta Metallurgica*, vol. 34, no. 3, pp. 497-510.
30. Erdogan, F. and Sih, G. C. (1963): "On the Crack Extension in Plates Under Plane Loading and Transverse Shear." *Journal of Basic Engineering*, vol. 85, no. 4, pp. 527.

STUDY OF CHARACTERISTICS OF INTERNAL SOLID-LIQUID TWO PHASE FLOW FIELD OF KYF FLOTATION MACHINE

Continued from page 633

(3) Mineral viscosity has great influence on the characteristics of internal flow field in flotation machine and minerals of higher viscosity are not good for the flotation separation of minerals.

Acknowledgment

The research work is supported by the National Natural Science Foundation of China (No.:51474087) and Hebei 100 Outstanding Innovative Talent Support Program (No.: BR2-214).

References

1. Shen, Z. C., Lu, S. J., Shi, S. X., Chen, D. and Yang, L. (2013): "Analysis and Discussion of Gas-Liquid Two Phases Flow Field of KYF Flotation Machine Based on CFD-Flow Field Measurement and Simulation Research on KYF Flotation Machine (□)," *Nonferrous Metals (Mineral Processing Section)*, No. 4, pp. 59-62, 2013.
2. Gui, X. H., Cheng, G., Liu, J. T., Li, S. L. and Wang, Y. T. (2012): "Process characteristics of heterogeneous fine mud in the coal flotation," *Journal of China Coal Society*, Vol. 37, No. 2, pp.301-309, 2012.
3. Yang, Y. J., Chen, J. H., Shen, Z. C. and Liao, X. (2015): "Simulation Study of the Flow Field Characteristics for Aeration Stirring Type Flotation Machine," *Conservation and Utilization of Mineral Resources*, No. 2, pp. 22-26, 2015.
4. Hu, M. Z., Chen, J. Q., Wu, B. Z. and Bu, X. Z. (2014): "Numerical Simulation on Flow Characteristics of Flotation Machine in Large Poor-tin Sulfide Ore," *Mining Research and Development*, Vol. 34, No. 7, pp. 71-74, 2014.
5. Koh, P. T. L. and Schwarz, M. P. (2008): "Modelling attachment rates of multi-sized bubbles with particles in a flotation cell," *Minerals Engineering*, Vol. 21, No. 12-14, pp. 989-993, 2008.
6. Shi, S. X., Zhang, M., Fan, X. S. and Chen, D. (2015): "Experimental and computational analysis of the impeller angle in a flotation cell by PIV and CFD," *International Journal of Mineral Processing*, Vol. 142, No. 10, pp. 2-9, 2015.
7. Su, M., Han, W., Zhang, Z., Li, R. and Li, Q. (2012): "Numerical Simulation and Analysis of Gas-Solid-Liquid Three-Phase Flow in Mechanical Flotation cell," *Procedia Engineering*, Vol. 31, pp. 850-856, 2012.
8. Tiitinen, J. (2003): "Numerical modeling of a OK rotor-stator mixing device," *Computer Aided Chemical Engineering*, Vol. 14, pp.959-964, 2003.
9. Xia, J. L., Rinne, A. and Gronstrand, S. (2009): "Effect of turbulence models on prediction of fluid flow in an Outotec flotation cell," *Minerals Engineering*, Vol. 22, No. 11, pp.880-885, 2009.
10. Li, R. N., Tang, K., Han, W., Li, Q. F. and Shen, J. F. (2009): "Numerical simulation of gas-liquid-solid three-phase inner flow in mechanically stirring air-charging flotation machine," *Journal of Lanzhou University of Technology*, Vol. 35, No. 1, pp.37-40, 2009.
11. Han, W., Li, R. N. and Yang, R. (2009): "Redesign of Mechanically Agitated Flotation Machine Based on InteriorFlow Fields Simulation," *Journal of Mechanical Engineering*, Vol. 45, No. 12, pp.84-88, 2009.
12. Zeng, K.W., Xue, Y. L. and Yu, Y. F. (2001): "Particle Velocity in the Three-phase Flow of Solid-liquid-gas in a Flotation Cell," *Metal Mine*, No. 5, pp.21-23, 2001.